Mon. Not. R. Astron. Soc. **000**, 000–000 (0000) Printed 1 February 2008 (MN LATEX style file v1.4)

Radio flares and plasmon size in Cygnus X-3

R. N. Ogley,[1,2⋆] S. J. Bell Burnell[1], R. E. Spencer[3], S. J. Newell[3], A. M. Stirling[4] and R. P. Fender[5]

[1] *Department of Physics and Astronomy, The Open University, Walton Hall, Milton Keynes, Buckinghamshire, MK6 7AA, UK*
[2] *Present address: Department of Physics, Keele University, Staffordshire, ST5 5BG, UK*
[3] *University of Manchester, Jodrell Bank Observatory, Macclesfield, Cheshire, SK11 9DL, UK*
[4] *CFA, University of Central Lancashire, Preston, PR1 2HE, UK*
[5] *Astronomical Institute 'Anton Pannekoek' and Center for High-Energy Astrophysics, University of Amsterdam, Kruislaan 403, 1098 SJ Amsterdam, the Netherlands*

1 February 2008

ABSTRACT

We have observed a number of minor radio flares in Cyg X-3 using the MERLIN array. Photometric observations show the system to be highly active with multiple flares on hourly timescales over the one month observing programme. Analysis of the source's power spectrum show no persistent periodicities in these data, and no evidence of the 4.8 hr orbital period. An upper limit of 15 mJy can be placed on the amplitude of any sinusoidal varaition of source flux at the orbital period. The brightness temperature of a flare is typically $T_{\rm b} \geq 10^9$-10^{10} K, with a number of small flares of 5 minute duration having brightness temperatures of $T_{\rm b} \geq$ few $\times 10^{11}$ K. For such a change in flux to occur within a typical 10 minute timescale, the radiation must originate from plasmons with a size ≤ 1.22 AU. This emission is unlikely to originate close to the centre of the system as both the jets and compact object are buried deep within an optically thick stellar wind. Assuming a spherically symmetric wind, plasmons would become visible at distances ~ 13 AU from the core.

Key words: binaries: close, stars: individual: Cyg X-3, stars: Wolf–Rayet, stars: variables: other, radio continuum: stars, X-rays: stars

1 INTRODUCTION

The energetic X-ray binary Cygnus X-3 has been studied in great detail since its discovery in 1967 (Giacconi et al. 1967). It is an active source with measurements in the radio, sub-mm, infrared, X-ray and gamma-rays all of which indicate a highly variable source.

Following infrared spectroscopic measurements (van Kerkwijk et al. 1992; Fender, Hanson & Pooley 1999), the accepted morphology of Cyg X-3 is a compact object in orbit around a Wolf-Rayet star of the WN4-5 type. A measured infrared and X-ray orbital period for the binary of 4.8 hr indicates a very compact system (≤ 10 R$_\odot$) within which a large degree of interaction takes place. The proximity of a compact object to a star with a strong wind provides both accretion onto the compact object, but also a medium of varying optical depth through which jets, formed from accreted material, must travel. Any emission from the jets cannot be observed directly until the wind becomes optically thin to the radiation in the jets. This creates a time-lag between radiation at different frequencies in the jet (typically radio and sub-mm emission) and between jet and central infrared and X-ray emission.

One can use the different radiation regimes to investigate different properties of the system. For example, the low-frequency radiation at radio and sub-mm frequencies comes from synchrotron emitting electrons in the jets, and this has been used by Ogley et al. (in prep.) to obtain an upper-limit to the magnetic field in the jets of 260 μT (2.60 G) at 100 R$_\odot$ from the core. As one observes higher frequencies, the emission changes from synchrotron to thermal free-free, which now comes from the wind in the system and not the jets. An example of the wind emission observed by the *ISO* satellite is given in Ogley, Bell Burnell & Fender (2001), and a complete spectrum showing the different emission mechanisms from radio to infrared is given in Ogley et al. (in prep.) Fig. 6. However, a thorough investigation using a single radiation regime can also provide a great deal of information.

The accretion process is not constant, but is probably variable in both density and mass-transfer rate. This causes a change in the number of electrons which are available for acceleration in the jet, which alters the synchrotron luminos-

⋆ E-mail: rno@astro.keele.ac.uk

ity. Radio photometry monitors the change in jet emission following a change in the Wolf–Rayet state and three distinct states of emission in the unresolved core of the system have been identified (Waltman et al. 1995):

(i) For the majority of the time the system is in a quiescent radio state with GHz flux densities around 100 mJy.

(ii) Once or twice a year the system undergoes a major flare. The radio flux density increases by 10-100 times on a timescale of around a day. A major flare is very energetic and lasts for days or weeks, exponentially decaying back to quiescence. Identified immediately before a major flare is a period of quenching during which the flux density drops to around 10 mJy and remains at this lower value for up to a week.

(iii) An intermediate state exists between the high flux of a major flare (> 1 Jy) and the normal quiescent flux of 100 mJy. This is the state of minor flaring and can last for several weeks. During a minor flare state, the system can undergo multiple short-duration flares and is highly active.

Continuous monitoring determines the radio state of Cyg X-3, and allows detailed investigation of the jet mechanism and structure during these different states.

2 THE RADIO OBSERVATIONS

Daily radio monitoring was carried out using the Ryle Telescope in Cambridge and the Green Bank Interferometer (GBI) in West Virginia. These observatories provided photometry at 2.3 and 8.3 GHz (GBI) and 15 GHz (Ryle). Identification of a minor flare in 1996 November triggered a set of interferometric observations using the MERLIN array. The MERLIN observations were scheduled at C-band (5 GHz) with 6 epochs of 12 hours in duration each separated by one week. The aim of these observations was to map the emission from a plasmon as it travelled from the centre of the binary, as observed by Newell (1995). At a frequency of 5 GHz a plasmon at 10 kpc, travelling at a speed of 0.35 c in the plane of the sky, would separate from the core at one MERLIN beam-width per epoch ($\simeq 50$ mas). This jet velocity, taken from the apparent transverse motion measured by Spencer et al. (1986) represents a lower-limit to the separation per epoch. Other measurements have indicated higher velocities of components close to the plane of the sky ($\simeq 0.6c$ from Martí et al. (2000) and $\simeq 0.8c$ from Mioduszewski et al. (2000)). These larger apparent velocities would therefore yield greater separations per MERLIN epoch.

Fig. 1 shows the radio photometry from the Ryle telescope at 15 GHz which was used as a trigger for the MERLIN observations. Cyg X-3 was in quiescence until MJD† 50400 when it underwent a mild quenching period (flux around 50 mJy). Shortly after the quenching, a minor flare occurred on MJD 50407 which signalled the start of a minor flare period. Subsequent minor flares occurred at random times after this date.

Observations were taken using the standard 5 GHz MERLIN continuum setup. A 15 MHz bandwidth was used for observations of the target source Cygnus X-3, a phase calibrator source 2005+403, a flux calibrator 3C84, and a point source calibrator, either OQ 208 or 0552+398. To calibrate the flux easily, observation of a point source of known flux is required. However, on the longer MERLIN baselines all the point sources are variable in flux, and all the constant flux sources are resolved. One has to observe a point source over all baselines and calibrate the flux scale by measurements of a source of known flux using the short baselines only. Details of this calibration procedure are given in the MERLIN user's guide, Thomasson et al. (1993) and Ogley (1998).

The source and observational details for all the epochs are given in Table 1. The times of the MERLIN observations are shown in Fig. 2 together with Ryle photometry at 15 GHz around the same time. The MERLIN observations are indicated by the arrows.

† In this paper we use the definition of modified Julian date to be MJD = JD − 2 400 000.5, so integer values of MJD fall on 0000 UT.

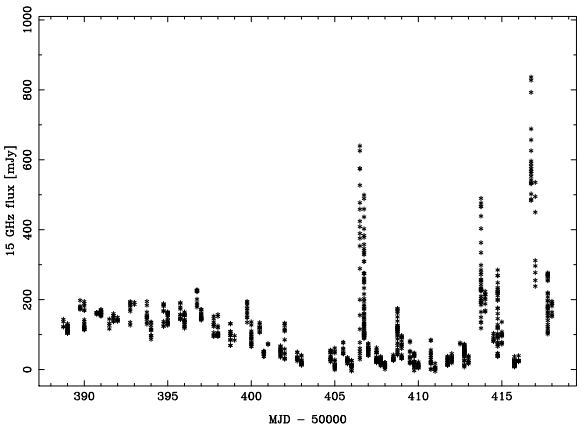

Figure 1. 15 GHz radio photometry from the Ryle telescope which triggered the start of our MERLIN observation programme. A minor flare occurred on MJD 50407 and our MERLIN observations were triggered from MJD 50419 until MJD 50459 as discussed in the text. See also Fig. 2.

Table 1. Date and calibration sources for the MERLIN observations.

		Calibrators	
MJD	Date	Point source, flux	Phase
50419	01 December 1996	OQ 208	2005+403
50425	07 December 1996	OQ 208	2005+403
50432	15 December 1996	0552+398	2005+403
50438	21 December 1996	OQ 208	2005+403
50446	28 December 1996	OQ 208	2005+403
50459	11 January 1997	0552+398	2005+403

3 MERLIN PHOTOMETRY

Because of the variable nature of the source at the time of the MERLIN observations, a robust map of the source is almost impossible to obtain. Variations in observed amplitude can be due to two things: a variable core; or emission away from the phase centre. To reconstruct an image,

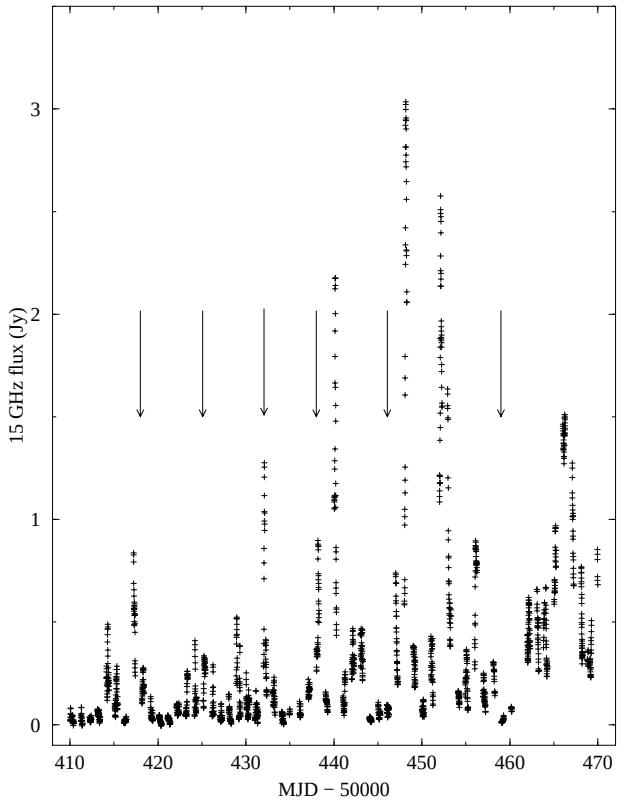

Figure 2. Times of the MERLIN observations indicated by arrows overlaying a plot of Ryle photometry at 15 GHz.

the assumption that any variation in the fringe amplitude with hour angle is due to the interferometer response to the source structure only is made. However, this is violated if the source varies within the time needed for aperture synthesis. For our observations, a direct reconstruction of the source results in many artifacts including jet-like emission from a central core. The variability of the source is shown in Fig. 3 which plots the measured flux against baseline length or *uv* spacing. One can see that the source is highly variable over all baseline distances and no accurate reconstruction of the source brightness distribution can be obtained.

The plot shown in Fig. 3 does allow some quantative evaluation. A resolved source would show a decrease in measured flux with increasing *uv* spacing, whereas during a flare the measured flux is approximately constant over all *uv* separations. In Fig. 3 the measured flux is high at the longest baselines suggesting that the source is unresolved. A source that is unresolved at a *uv* spacing of 3.5 Mλ at 5 GHz has an angular size of less than 70 mas. This is consistent with a scatter-broadened size of Cygnus X-3, which has a strong dependence on frequency (Wilkinson, Narayan & Spencer 1994) and has been measured at 5 GHz to be $\simeq 20-30$ mas (Mioduszewski et al. 2000).

For these observations the success of the MERLIN array is not in its imaging capabilities, but its photometry. Figs 4-9 show photometry for all six C-band epochs. Note that in these figures the vertical scales vary and the zero is not included. Vertical lines in all these figures indicate the time at which X-ray minimum occurs using the ephermeris by Matz et al. (1996). Data have been averaged into time bins

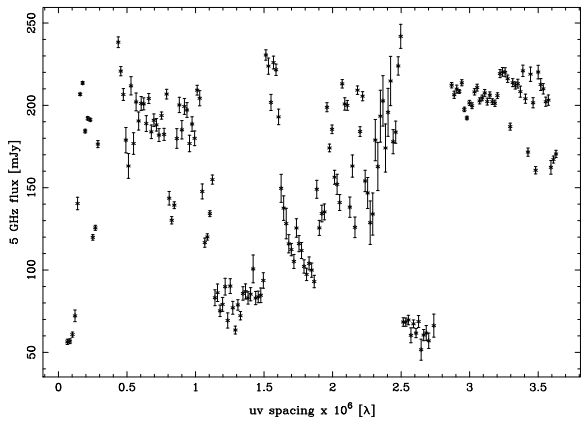

Figure 3. A plot of flux against *uv* distance for the entire first epoch. There is significant, and unstructured, variation of flux which is unlikely to be caused by source structure and is due to changes in the source flux over the epoch.

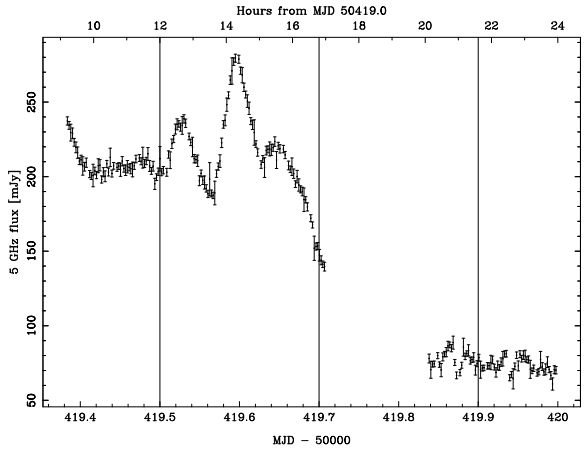

Figure 4. Cyg X-3 photometry on 01 December 1996. Time bins are 3.4 min. Vertical lines indicate time of X-ray minimum from the ephermeris by Matz et al. (1996).

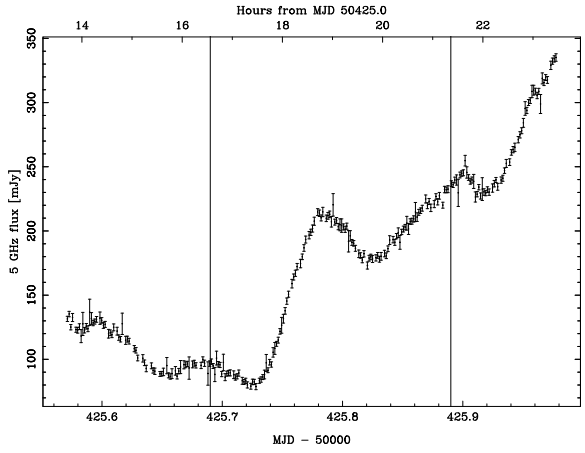

Figure 5. Cyg X-3 photometry on 07 December 1996. Time bins are 2.2 min.

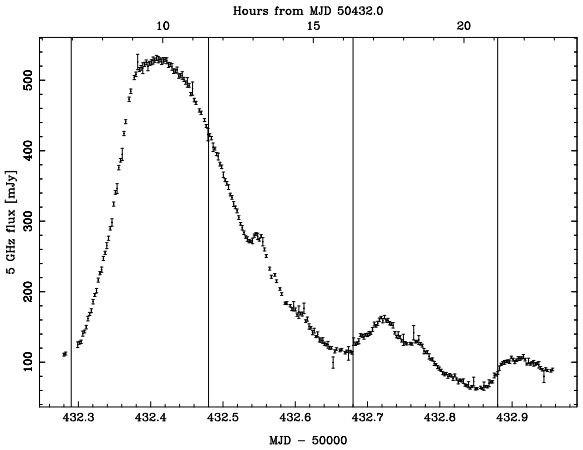

Figure 6. Cyg X-3 photometry on 15 December 1996. Time bins are 3.8 min.

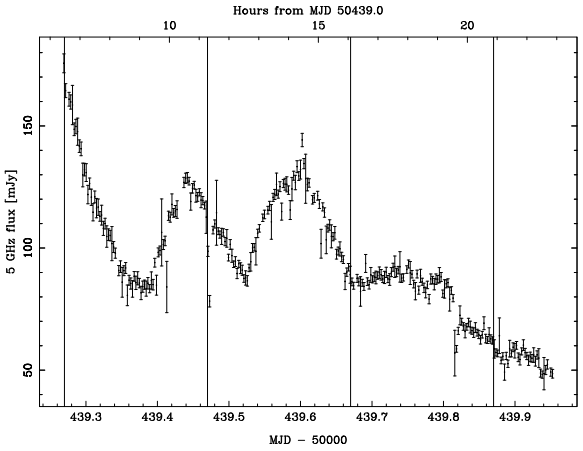

Figure 7. Cyg X-3 photometry on 21 December 1996. Time bins are 4.0 min.

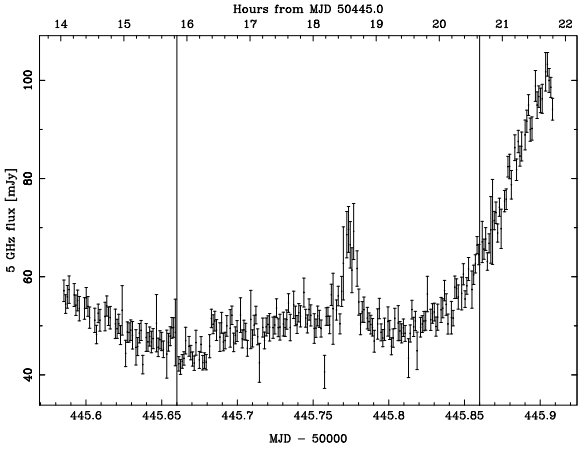

Figure 8. Cyg X-3 photometry on 28 December 1996. Time bins are 2.0 min.

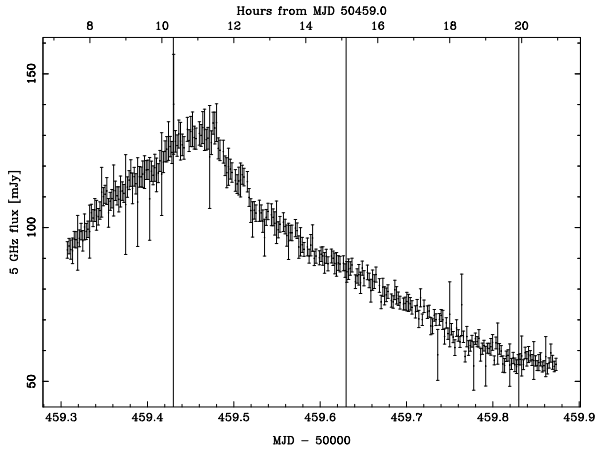

Figure 9. Cyg X-3 photometry on 11 January 1997. Time bins are 3.4 min.

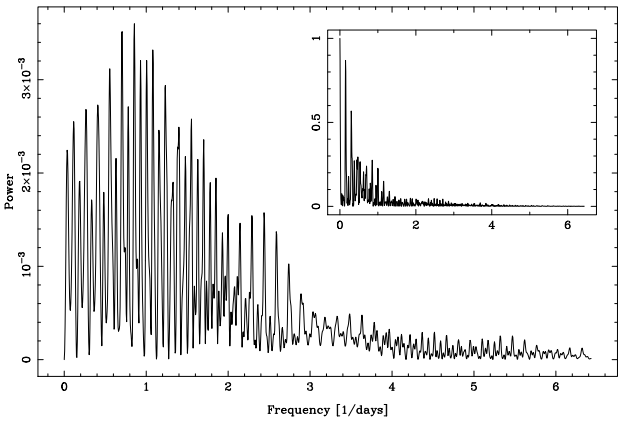

Figure 10. A raw power spectrum from all six epoch photometric points. The insert is the Fourier transform of the sampling function of the data.

of 2.0-4.0 minute duration to reduce noise and all baselines have been used.

A number of features are visible in the plots. Points to note in the data are:

(i) In all but the first four hours of the MJD 50445 (28 December 1996) observation, the flux is variable on timescales shorter than a couple of hours. This causes problems in the mapping as discussed above.

(ii) A number of flares occurred, however, the timescales involved are not constant or correlated with flare strength or length of time in quiescence preceding a flare.

3.1 Power spectra

To search for any periodic signals in the data, photometric points from all six epochs were included and the Fourier spectrum was determined. This is shown in Fig. 10. The main part of the figure is a direct Fourier transform of the data. The insert is the Fourier transform of the windowing function.

The main transform of the data is the time-domain

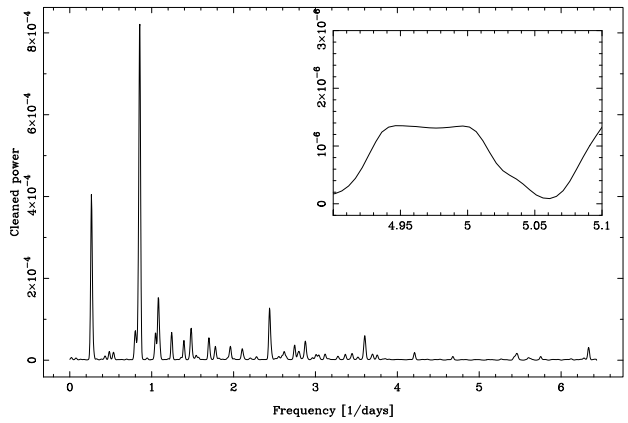

Figure 11. A cleaned spectrum. The insert shows the power at a period of 4.8 hours. There is no evidence for any periodic signal at this binary period.

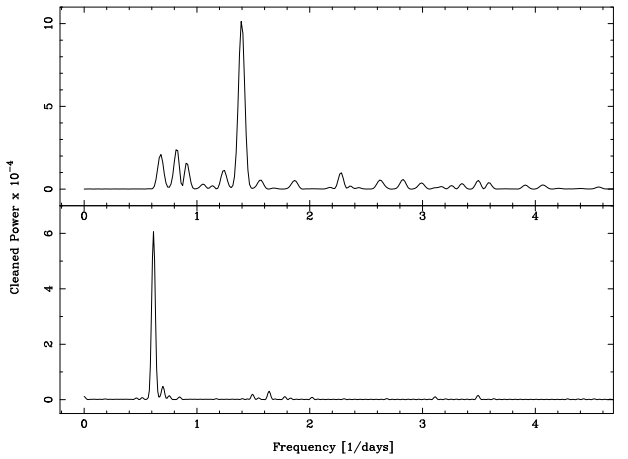

Figure 12. Power spectra of the data cleaned in an identical way to Fig. 11, but split into two halves. The top panel shows the first three epochs, and the bottom panel shows the latter three epochs. No correlation in the periods are found between the two halves of the data.

equivalent of an interferometric dirty map, and the transform of the windowing function is the equivalent of a dirty beam. In the same way as one can re-create a clean map from a dirty map and dirty beam, the power spectrum can be cleaned by an iterative subtraction of the window function (Clark 1980; Roberts, Lehar & Dreher 1987). The result of this procedure is shown in Fig. 11.

To check whether the periods shown in Fig. 11 are spurious, the first three epochs were analysed separately from the last three epochs. The clean spectra are shown in Fig. 12. As there is no correlation between the two halves of the data sets, we can conclude that there are no stable periodicities and any periodicity shown is due to spurious features or quasi-periodic oscillations.

4 DISCUSSION

4.1 Brightness temperature of the flares

A brightness temperature of a flare can be calculated associated with the flux change from the source. A black body sphere with radius r, flux S_ν, at a distance D, assuming a Rayleigh-Jeans tail, would have a brightness temperature of

$$T_{\rm b} = \frac{c^2 S_\nu D^2}{2k_{\rm B}\nu^2 r^2} \tag{1}$$

where c is the speed of light, $k_{\rm B}$ is Boltzmann's constant and ν is the frequency. Therefore a flare of duration Δt minutes and flux change of ΔS mJy has a brightness temperature of

$$T_{\rm b} = 9.66 \times 10^{10}\ \frac{\Delta S_{\rm mJy} D^2_{\rm kpc}}{\nu^2_{\rm GHz}\Delta t^2_{\rm min}}\ \ {\rm K} \tag{2}$$

where quantities are measured in their subscripted units.

For a typical flare: MJD 50419.56, the flux increase $\Delta S = 80$ mJy over $\Delta t = 46$ minutes at $\nu = 5$ GHz. If Cyg X-3 is at a distance of 10 kpc, the brightness temperature is $T_{\rm b} \geq 1.5 \times 10^{10}$ K. This value is typical for the majority of flares, including the large flare at MJD 50432. The largest brightness temperature occurred at MJD 50438.6, if the change within 1 integration bin is believable. For this flare the flux change is $\Delta S = 10$ mJy over $\Delta t = 4.0$ min, and so the brightness temperature is $T_{\rm b} \geq 2 \times 10^{11}$ K.

There is a maximum brightness temperature above which inverse Compton losses become catastrophic. This maximum brightness temperature can be written for galactic sources as

$$T_{\rm max} \leq 1.6 \times 10^{12}\ \left(c_{56}^{(\alpha)}\right)^{0.8} \left(\frac{(1-\alpha)}{\nu_U}\left[\frac{\nu_U}{\nu}\right]^{\alpha}\right)^{0.2} \mathcal{D}^{1.2}, \tag{3}$$

where ν_U is the upper frequency of the synchrotron emission in GHz, $\mathcal{D}$ is the Doppler boosting factor of the emission and $c_{56}^{(\alpha)}$ is the α-dependent parts of the ratio of Pacholczyk constants c_5 and c_6 where

$$c_{56}^{(\alpha)} = \frac{3\alpha+5}{6\alpha^2+19\alpha+13}\frac{\Gamma\left(\frac{3\alpha+1}{6}\right)\Gamma\left(\frac{3\alpha+5}{6}\right)}{\Gamma\left(\frac{6\alpha+5}{12}\right)\Gamma\left(\frac{6\alpha+13}{12}\right)}. \tag{4}$$

(Pacholczyk 1970; Hughes & Miller 1991). For a spectral index of $\alpha = -0.1$, and $\nu_U = 350$ GHz (Ogley et al. in prep.), and a frequency of $\nu = 5$ GHz used in this work, the expression for the maximum brightness temperature evaluates to

$$T_{\rm max} \leq 4.8 \times 10^{11} \mathcal{D}^{1.2}\ \ {\rm K}. \tag{5}$$

An estimation of the bulk Doppler factor of the jets can be inferred from jet expansion. An arcsec-scale measurement (Martí et al. 2000) has shown that at that distance from the core, components are expanding with proper motions of $\mu_a = 10.9$ mas d^{-1} and $\mu_r = 9.8$ mas d^{-1} for the approaching and receding components respectively. This allows an estimate of the jet bulk velocity and angle to the line of sight to be measured, where

$$\beta\cos\theta = \frac{\mu_a - \mu_r}{\mu_a + \mu_r}. \tag{6}$$

From these observations the authors find $\beta\cos\theta = 0.053 \pm 0.027$, from which they assume a jet velocity of $\beta = 0.60$ and an angle to the line of sight of $\theta = 85°$. If these values are adopted then a Doppler factor of $\mathcal{D} = 1.18$ can be calculated. If the jet speed is increased to $\beta = 0.89$ as observed in VLBA

observations (Mioduszewski et al. 2000), then by using the same value of θ, the Doppler factor increase to $\mathcal{D} = 2.02$. Using this range of Doppler factors, the maximum brightness temperature is therefore $T_{\rm max} \leq 6 - 11 \times 10^{11}$ K.

4.2 Orbital motion

The effect of the binary's orbital motion on the observed radio emission from Cyg X-3 is found to be negligible, unlike Cyg X-1 (Brocksopp et al 1999). Reasons why this could be are

(i) The binary is face on (which is irrespective of the jet angle). Throughout the orbit there is no difference in the amount of material that the jets encounter which would scatter or absorb radiation.
(ii) Radio emission in Cyg X-3 is dominated by optically thin events which occur from a region way outside the orbital diameter, and so any 4.8 h variation, in say particle production or blob ejection, is smoothed out by the time we see it. In Cyg X-1, the radio emission is self-absorbed and is dominated by the high frequencies, this occurring closer to the binary centre.

To quantify this absence of radio emission, each run was Fourier transformed into 100 frequencies with a separation of 0.1 cycles per day. The power spectra were then summed over all the data sets. No significant peak at or around 5 cycles per day ($\equiv$ 4.8 h period) was found in either the individual spectra or in the sum. A 2 σ upper limit of 15 mJy can be set for the amplitude of any sinusoidal variation in source flux for the average power spectrum. Each daily run was also split into 5 overlapping data sets, transformed and averaged to give an average power sepctrum per run. These showed significantly higher power at low frequencies with a power-law dependence with a typical slope of -2.4 ± 0.2 over the frequency range 4–40 cycles per day. The power law shows that no particular timescale can be assigned to the data.

We have indicated on the figures 4 – 9, by vertical lines, the times of X-ray orbital minimum as calculated from the ephemeris of Matz et al. (1996), and one can see that any radio state is equally probable.

4.3 Emission position

From the small time-scale variations in the photometric data flares can be identified as originating from a region typically 10 light minutes, or 1.22 AU across. However, it is highly unlikely that this emission occurs close to the centre of the system where the jets are accelerated, as both the jets and the compact object are buried deep within an optically thick, dense stellar wind from the companion star, see Ogley, Bell Burnell, Fender (2001).

The varying opacity to the radiation from the wind creates zones along the jet where radiation at different frequencies dominates, as the surrounding medium becomes optically thin. Radii at which this occurs can be calculated using a modified Wright & Barlow (1975) wind model, a function for the Gaunt factor appropriate for radio wavelengths (Leitherer & Robert 1991) and assuming spherical symmetry. The radius at which emission occurs then depends on only the wind parameters such as composition, temperature and mass-loss rate, as well as the frequency of the observed emission. From the delay of flares at 2.25, 8.3 and 15 GHz during 1991 to 1995, parameters for the mean number of free electrons, $\gamma = 1$, the RMS ionic charge, $Z = 1$, the mean atomic weight per nucleon, $\mu = 4$, the temperature, $T = 20,000$ and the mass-loss rate, $\dot{M} = 1 \times 10^{-5}$ M$_\odot$ yr^{-1} can be calculated (Waltman et al. 1996). This then simplifies the frequency-dependent radius to

$$R_c = 3.28 \times 10^3 \; g^{1/3} \nu_{\rm GHz}^{-2/3} \;\; {\rm R}_\odot, \tag{7}$$

where

$$g = 9.77 + 1.27 \; \log \left(2.83 \times 10^3 \; \nu_{\rm GHz}^{-1} \right) \tag{8}$$

and $\nu_{\rm GHz}$ is the frequency measured in GHz. For a frequency of 5 GHz, the radius at which emission is observed is therefore $R_c \geq 13$ AU. This creates significant layering in the emission from the jets with the higher frequencies occurring closer to the centre (at 350 GHz, emission would occur at only 0.5 AU; see Ogley et al. in prep.). We note that the Waltman et al mass loss rate assumes an expansion velocity of only 0.3c; a higher velocity would give a larger mass loss rate and larger values of R_c. Furthermore Ogley et al (2001) find a significantly larger mass loss rate from infrared observations, a rate independent of the expansion velocity. Finally we note that the wind may not be spherically symmetric - see Ogley, Bell Burnell, Fender (2001) and Fender, Hanson, Pooley (1999).

5 CONCLUSIONS

We have observed the X-ray binary Cygnus X-3 with the MERLIN interferometer with the intention of mapping jet components in a period of minor flare activity. We observed for six epochs between 01 December 1996 and 11 January 1997. In all epochs the source showed some degree of variability and consequently we were unable to map the source without the creation of artifacts.

High time-resolution photometric observations show a number of small-flux flares of around an hour in duration, with a large amount of structure. This is typical of a minor-flare period. Power spectra of the data show no persistent periodicities in the data, and no evidence of the orbital period of 4.8 hr.

A measurement of the brightness temperature for the flares show typical values of 10^9-10^{10} K, with the largest values occurring over 4 minutes and a brightness temperature of 2×10^{11} K. The flare emission is from a region of typically 10 light minutes across, with a diameter of 1.22 AU. However, to be visible at a frequency of 5 GHz these plasmons would be situated at a distance of 13 AU from the core, assuming a spherical wind.

6 ACKNOWLEDGMENTS

The Authors wish to thank various MERLIN staff for help with data and analysis. We are grateful for the help given by Tom Muxlow, Simon Garrington and Peter Thomasson for scheduling the observations and giving advice in the data

reduction. The authors also wish to thank Duncan Law-Green for his assistance in attempting to map the data. RNO wishes to thank Patrick McGrough and Robin Sanderson for their hospitality during the writing of this paper.

Guy Pooley generously made available the Ryle Telescope data.

The Green Bank Interferometer is a facility of the National Science Foundation operated by the NRAO in support of NASA High Energy Astrophysics programme. MERLIN is a National Facility operated by the University of Manchester on behalf of PPARC.

REFERENCES

Brocksopp C., Fender R.P., Larionov V., Lyuty V.M., Tarasov A.E., Pooley G.G., Paciesas W.A., Roche P., 1999, MNRAS, 309, 1063

Clark B.G., 1980, A&A, 89, 377

Fender R.P., Hanson M.M., Pooley G.G., 1999, MNRAS, 308, 473

Giaconni R., Gorenstein P., Gursky H., Waters J, 1967, ApJ, 273 L119

Hughes P.A., Miller L., 1991, Beams and Jets in Astrophysics, Cambridge Astrophysics Series, 19, Chapter 1, 33

Leitherer C., Robert C., 1991, ApJ, 377, 629

Martí, J., Paredes J.M., Peracaula M., 2000, ApJ, 545, 939

Matz S. M., Fender R.P., Bell Burnell S.J., Grove J.E., Strickman M.S., 1996, A&AS, 120, 235

Mioduszewski A.J., Rupen M.P., Hjellming R.M., Pooley G.G., Waltman E.B., 2001, ApJ in press, astro-ph/0102018

Newell S.J., 1995, PhD thesis, The University of Manchester

Ogley R.N., 1998, PhD thesis, The Open University

Ogley R.N., Bell Burnell S.J., Fender, R.P., 2001, MNRAS, 322, 177

Pacholczyk A.G., 1970, Radio Astrophysics, W.H. Freeman and Co., San Francisco

Roberts D.H., Lehar J., Dreher J.W., 1987, AJ, 93, 968

Spencer R.E., Swinney R.W., Johnston K.L., Hjellming R.M., 1986, ApJ, 309, 707

Thomasson P., Garrington S.T., Muxlow T.W.B., Leahy J.P, 1993, MERLIN user's guide, The University of Manchester

van Kerkwijk M.H., Charles P.A., Geballe T., King D., Miley G., Molar L., van den Heuvel E., van der Klis M., van Paradijs J., 1992, Nat, 355, 703

Waltman E.B., Ghigo F.D., Johnston K.L., Foster R.S., Fielder R.L., Spencer J.H., 1995, AJ, 110, 290

Waltman E.B., Foster R.S., Pooley G.G., Fender R.P., Ghigo F.D., 1996, AJ, 112, 2690

Wilkinson P.N., Narayan R., Spencer R.E., 1994, MNRAS, 269, 67

Wright A.E., Barlow M.J., 1975, MNRAS, 170, 41